Cell, Vol. 122, 351–363, August 12, 2005, Copyright ©2005 by Elsevier Inc. DOI 10.1016/j.cell.2005.07.014

Allosteric Modulation of the RNA Polymerase Catalytic Reaction Is an Essential Component of Transcription Control by Rifamycins

Irina Artsimovitch,[1] Marina N. Vassylyeva,[2] Dmitri Svetlov,[1] Vladimir Svetlov,[1] Anna Perederina,[2] Noriyuki Igarashi,[4] Naohiro Matsugaki,[4] Soichi Wakatsuki,[4] Tahir H. Tahirov,[3] and Dmitry G. Vassylyev[2,5,*]

[1]Department of Microbiology
The Ohio State University
484 West 12th Avenue
Columbus, Ohio 43210

[2]Structural and Molecular Biology Laboratory

[3]High Throughput Factory RIKEN Harima Institute at Spring-8
1-1-1 Kouto, Mikazuki-cho, Sayo, Hyogo 679-5148
Japan

[4]Structural Biology Research Center
Photon Factory
Institute of Materials Structure Science
High Energy Accelerator Research Organization (KEK)
1-1 Oho, Tsukuba, Ibaraki, 305-0801
Japan

[5]Department of Biochemistry and Molecular Genetics
University of Alabama at Birmingham
Schools of Medicine and Dentistry
502 Kaul Genetics Building
720 20th Street South
Birmingham, Alabama 35294

Summary

Rifamycins, the clinically important antibiotics, target bacterial RNA polymerase (RNAP). A proposed mechanism in which rifamycins sterically block the extension of nascent RNA beyond three nucleotides does not alone explain why certain RNAP mutations confer resistance to some but not other rifamycins. Here we show that unlike rifampicin and rifapentin, and contradictory to the steric model, rifabutin inhibits formation of the first and second phosphodiester bonds. We report 2.5 Å resolution structures of rifabutin and rifapentin complexed with the *Thermus thermophilus* RNAP holoenzyme. The structures reveal functionally important distinct interactions of antibiotics with the initiation σ factor. Strikingly, both complexes lack the catalytic Mg^{2+} ion observed in the apo-holoenzyme, whereas an increase in Mg^{2+} concentration confers resistance to rifamycins. We propose that a rifamycin-induced signal is transmitted over 19 Å to the RNAP active site to slow down catalysis. Based on structural predictions, we designed enzyme substitutions that apparently interrupt this allosteric signal.

Introduction

Bacterial RNAP holoenzyme, composed of a catalytic core ($\alpha_2\beta\beta'\omega$ subunits) and a σ-specificity factor, binds to a promoter and initiates reiterative abortive synthesis of short RNA products. Once a stable, ≥8 nt-long RNA primer is synthesized to form an 8–9 bp RNA/DNA hybrid, RNAP leaves the promoter and enters a highly processive elongation state that persists for thousands of nucleotide addition cycles. Rifamycins (Rifs) that were discovered nearly 50 years ago as fermentation by-products of *Streptomyces mediterranei* sp. (for a comprehensive review, see Floss and Yu, 2005) strongly inhibit synthesis of short RNAs but do not affect stable transcription elongation complexes (Sippel and Hartmann, 1970).

Rifamycins still retain their prominence as the first-line antibiotics in combating tuberculosis; however, their efficiency and versatility is limited by the rapid emergence of resistant bacteria. To overcome this problem, one needs to understand the detailed mechanisms of both the Rifs' action and the bacterial resistance to these drugs. Rifs belong to a group of ansamycin antibiotics that contain an aromatic naphthoquinone moiety (ansa ring) with a variable "tail" attached to the C3 and/or C4 positions (Figure 1A). The range of antibacterial activity for different C3/C4-substituted Rifs can easily span several orders of magnitude (Maggi et al., 1965). Therefore, it is not surprising that most of the efforts in drug design were concentrated on the creation of new C3/C4 substituted variants. Three Rifs are currently used in therapy: rifampicin (RFP), rifapentin (RPN), and rifabutin (RFB). However, functional in vitro analysis of the inhibitory mechanism focused only on RFP. The structure of the *Thermus aquaticus* core RNAP (taqRNAP) in complex with RFP determined at 3.3 Å resolution (Campbell et al., 2001) showed that, in support of genetic data (Boyd and Zillig, 1974; Jin and Gross, 1988; Kawai et al., 1976; Ovchinnikov et al., 1983; Severinov et al., 1993, 1994), RFP binds to a site on the β subunit located in the path of the nascent RNA. This suggested an intuitive and simple model in which RFP sterically blocks synthesis of an RNA product longer than 3 nt, and all β substitutions that confer resistance to RFP do so by distorting its binding pocket.

However, several observations cannot be easily reconciled with the simple steric hindrance mechanism (Table 1). Some of these discrepancies could be due to the fact that the structure was obtained with a non-physiological RFP target (core enzyme); indeed, cross-linking of the Rif tail to the σ subunit has been reported (Mustaev et al., 1994; Stender et al., 1975). Most importantly, this model fails to account for the existence of *rpoB* mutants that are resistant to RFP and RPN yet sensitive to RFB in vivo (Wichelhaus et al., 2001; Williams et al., 1998) since the tail, the only variable part of the compounds tested, does not make any contacts to RNAP (Campbell et al., 2001). Interestingly, substitutions that confer differential sensitivity phenotypes cluster far from the tail in the structure.

In order to resolve these lingering disparities, we pursued three parallel approaches: structural, biochemical, and genetic. First, we demonstrated that the tails confer differential effects on transcription in vitro. Second, we have determined the high-resolution structures

*Correspondence: dmitry@uab.edu

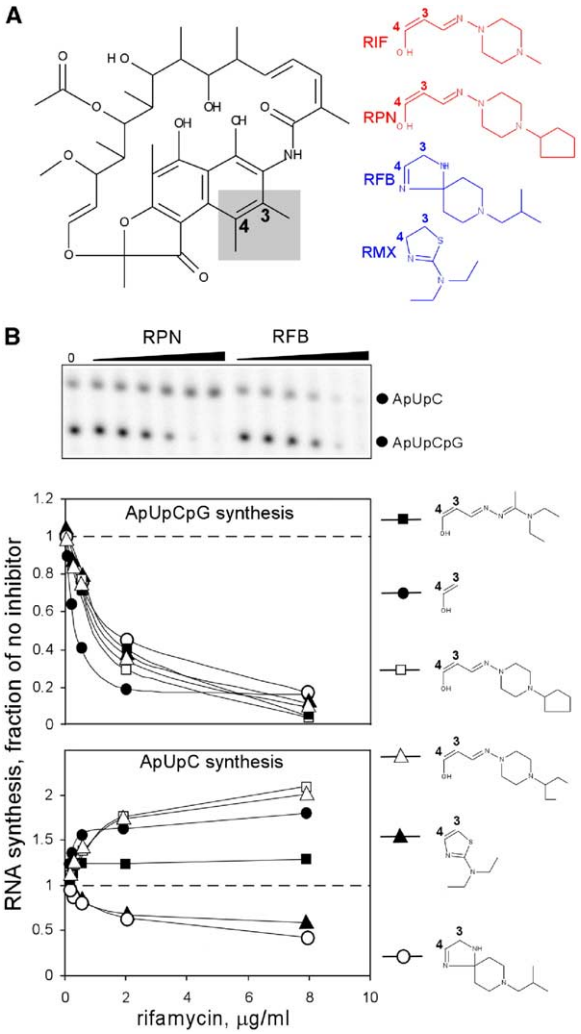

Figure 1. Inhibition of *E. coli* RNAP by Rifs In Vitro Depends on Their Mode of Tail Attachment

(A) Two classes of rifamycins with tails attached to C3 (red, RFP—rifampicin, RPN—rifapentin) and C3/C4 (blue, RFB—rifabutin, RMX—rifamexyl) positions of the ansa ring (naphtohydroquinonic chromophore spanned by an aliphatic bridge).

(B) RNA synthesis as a function of Rifs' concentrations. (Top) A representative gel panel, (bottom) effects of Rif tail (shown on the right) on ApUpCpG and ApUpC synthesis. The error bars are omitted for clarity; the error was within 10% between three independent titrations.

of RPN and RFB in complex with the *T. thermophilus* RNAP holoenzyme (ttRNAP) and performed systematic analysis of Rif-RNAP contacts. Third, we showed that distinct contacts of RPN and RFB tails to σ correlated with their patterns of RNAP inhibition. While our data do not exclude the steric model as a critical step of the Rifs' inhibition mechanism, they argue that Rifs also inhibit transcription at earlier steps through an allosteric signal that disfavors binding of the Mg^{2+} ion in the active site, thus slowing down catalysis and facilitating dissociation of short RNA transcripts. This model adequately explains observations that are at odds with the steric-block mechanism.

Results and Discussion

Different Mode of Tail Attachment Confers Differential Effects on Transcription

Differential bactericidal effects of Rif tails were thought to result from different permeability of bacterial cell walls to individual rifamycins (Brufani et al., 1982). However, direct differential effects on transcription were also noted (Wehrli and Staehelin, 1969). In order to directly assess the impact of tail variations, we compiled a set of rifamycins that differ in the structure and position of tail attachment and tested their effects on transcription by *E. coli* RNAP in vitro (Figure 1B). Consistent with previous reports (McClure and Cech, 1978), RFP inhibited the formation of the *second* phosphodiester bond when transcription was initiated with ApU dinucleotide and thus led to a decrease in ApUpCpG synthesis but did not inhibit the ApUpC synthesis. This pattern of inhibition is shared by all rifamycins tested with tails attached to C3 (Figure 1B and data not shown). In contrast, RFB and rifamexyl (RMX), whose tails are attached to C3/C4 positions, inhibited even the *first* phosphodiester bond formation (Figure 1B).

Structures of RNAP/Rif Complexes

To ascertain whether structurally different Rifs make distinct contacts with the enzyme, we obtained crystals of ttRNAP holoenzyme with Rifs from each class, RPN and RFB. We chose RPN for structural studies because of its greater stability in solution and because we did not detect any qualitative or quantitative differences between RFP and RPN in either in vivo or in vitro assays. Though the crystals used in these studies were obtained in the same crystallization conditions and belonged to the same space group as the previously reported structures, they exhibited a substantial increase (~2%) in all unit cell parameters that make them nonisomorphous with the previous crystals (Vassylyev et al., 2002). To ensure adequate comparison of the ttRNAP/Rif complexes with the apo-holoenzyme, we collected diffraction data and refined the structure of the native apo-holoenzyme in this crystal form at 2.8 Å

Table 1. Observations that Cannot Be Easily Explained by the Steric Block Model

Observation	Reference
Inhibition of the first phosphodiester bond formation	McClure and Cech, 1978
RFP-resistant substitutions distant from the inhibitor binding site	Jin and Gross, 1988
Inhibition of GreA-facilitated cleavage and pyrophosphorolysis in binary complexes by RFP	Altmann et al., 1994
β substitutions that are resistant to RFP and RPN but sensitive to RFB	Wichelhaus et al., 2001; Williams et al., 1998
Differential RFP resistance of holoenzymes containing σ^{70} and σ^{32} initiation factors	Wegrzyn et al., 1998

Table 2. Data Collection and Refinement Statistics

	Apo-holoenzyme	RNAP/RPN	RNAP/RFB
Space group		$P6_5$[a]	
Unit cell parameters (Å)		$a = b = 239.5$, $c = 253.1$	
Resolution (Å)	25.0–2.8 (2.90–2.80)[b]	25.0–2.5 (2.59–2.50)	25.0–2.5 (2.59–2.50)
Reflections (Total/Unique)	562759/184546	876633/260112	727855/257186
I/σI	25.2 (2.7)	20.2 (2.3)	17.2 (2.3)
R_{merge}	6.6 (43.6)	6.5 (46.3)	7.4 (43.8)
Completeness (%)	92.0 (77.5)	92.6 (72.4)	91.2 (78.8)
Refinement			
Space group		$P3_2$	
Resolution (Å)	25.0–2.8 (2.90–2.80)[b]	25.0–2.5 (2.59–2.50)	25.0–2.5 (2.59–2.50)
Reflections used	366401	517106	511160
R factor (%)	23.1 (32.7)	23.0 (33.9)	22.5 (31.7)
R_{free} (%)	26.8 (36.5)	26.7 (35.6)	25.7 (34.5)
RMSD bond length (Å)	0.016	0.016	0.015
RMSD bond angles (°)	1.90	1.88	1.86
RMSD improper angles (°)	1.10	1.10	1.10
Number of protein atoms	53574	53574	53574
Number of water molecules	5117[c]	6399	6845
Number of rifamycins' atoms	0	126	122
Number of active-site Mg^{2+} ions	2	0	0
Number of other Mg^{2+} ions	0[d]	487	562
Number of Zn^{2+} ions	4	4	4

$R_{merge} = \Sigma_{hkl}\Sigma_j|I_j(hkl) - \langle I(hkl)\rangle|/\Sigma_{hkl}\Sigma_j \langle I(hkl)\rangle$, where $I_j(hkl)$ and $\langle I(hkl)\rangle$ are the intensity of measurement j and the mean intensity for the reflection with indices hkl, respectively. R factor, $_{free}=\Sigma_{hkl}||F_{calc}(hkl)| - |F_{obs}(hkl)||/\Sigma_{hkl}|F_{obs}|$, where the crystallographic R factor is calculated including and excluding reflections in the refinement. The free reflections constituted 4% of the total number of reflections. RMSD—root mean square deviation. I/σ(I)—ratio of mean intensity to a mean standard deviation of intensity.

[a] The crystals belong to $P3_2$ space group with a perfect (50%) merohedral twinning mimicking $P6_5$ space group. The data were therefore processed in $P6_5$ space group and were expanded to $P3_2$ space group for refinement.

[b] The data for the highest resolution shell are shown in brackets.

[c] The water molecules were added by the standard alternating cycles of the water pick (water molecules were picked at 3σ level in the difference $|F_{obs} - F_{calc}|$ ED map) and water delete (water molecules with correlation coefficients less than 0.45 and peak heights less than 1.25σ in the $|2F_{obs} - F_{calc}|$ ED map were deleted) procedures. The water molecules were added until R_{free} dropped by less than 0.5% at the last cycle. A relatively large number of water molecules may account for a large solvent content of the crystal (~77%) and also for very mild, nearly physiological conditions at which crystals were grown that might allow better specific hydration of the RNAP molecules.

[d] The water molecules with low B factor values (< 20 $Å^2$), characterized by more than 5σ level in the |2Fo–Fc| ED map and having at least one oxygen ligand, were converted into Mg^{2+} ions for the RNAP/Rifs complexes but were not included in the native holoenzyme structure in view of the lower resolution of the diffraction data.

resolution (R factor = 23.1%, R_{free} = 26.8%) in addition to the RNAP/RPN (R factor = 23.0%, R_{free} = 26.7%) and RNAP/RFB (R factor = 22.5%, R_{free} = 25.7%) structures refined at 2.5 Å resolution (Table 2 and Figure S1). This crystal form exhibited only one significant difference from published ttRNAP structures—the bridge helix was uniform (straight), in contrast to the previously observed, locally distorted (with the two residues flipped out of the helix) conformation (Vassylyev et al., 2002). This difference, however, was observed in all three structures and therefore cannot be attributed to the Rifs' binding (Supplemental "RNAP structure").

As the uniform conformation of the bridge was previously observed only in eukaryotic RNAP, the finding that both conformations can exist in the same (bacterial) system further supports the earlier hypothesis that the local flipping of the bridge helix is universal for multisubunit RNAPs and may mediate DNA translocation during transcription (Cramer et al., 2001; Vassylyev et al., 2002).

Both RNAP/Rif complexes contained two molecules in the asymmetric unit designated as RNAP1 and RNAP2, as observed previously (Artsimovitch et al., 2004; Vassylyev et al., 2002). Surprisingly, although high concentrations of magnesium formate (~15 mM) and a nearly physiological pH (6.5) were used for crystallization, the high-affinity Mg^{2+} ion, bound to the catalytic β' Asp residues (positions 460, 462, and 464; throughout the text, the *Escherichia coli* numbering is used) was absent from all four independent RNAP molecules from the two Rif complexes. In contrast, this ion was observed in all previous multisubunit RNAP structures, as well as in isomorphous apo-holoenzyme crystals as revealed by the difference electron density (ED) built using $|F_{nati} - F_{rif}|$ coefficients, where F_{nati} and F_{rif} are the structure factors for the apo-holoenzyme and Rif complexes, respectively, and the phases are from the partially refined apo-holoenzyme structure (Figure 2A). The same phases, but with reversed $|F_{rif} - F_{nati}|$ coefficients, revealed the clear ED for RPN and RFB (Figures 2B and 2C) that allowed unambiguous fit of the antibiotics in the complexes. RPN and RFB bound to the same site on ttRNAP as did RFP in the taqRNAP/RFP complex (Campbell et al., 2001), with positions and contacts of the two ansa rings nearly superimposable (Figure 2D).

Rifamycins' Binding to RNAP

The Rif binding site is highly conserved among bacteria: amino acid sequences in the vicinity of the Rif contacts are identical between *T. thermophilus* and *T. aquaticus* RNAPs, whereas the evolutionarily distant *E. coli* sequence is 82% identical and 90% homologous to

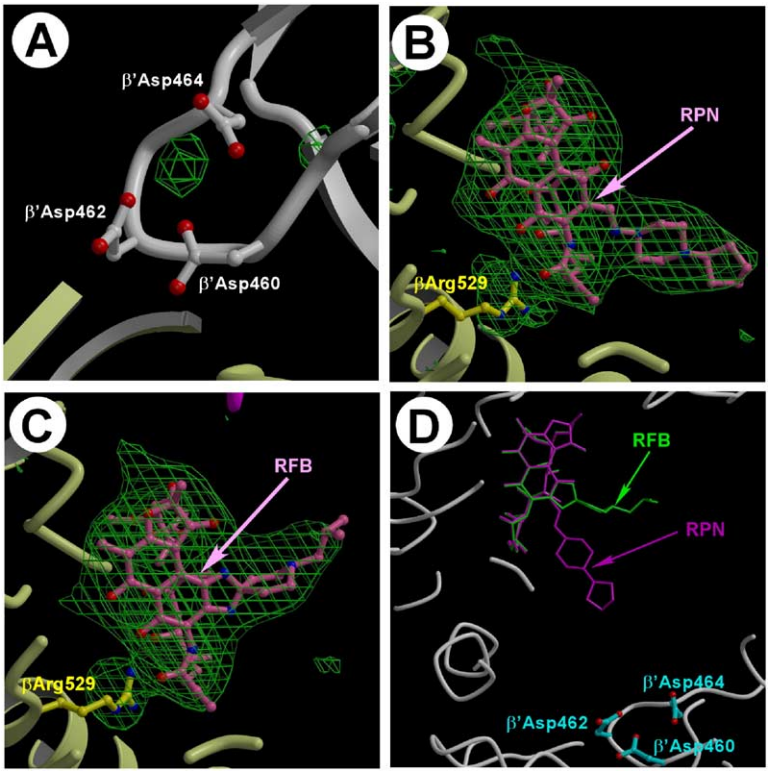

Figure 2. The Structures of RNAP/Rifs Complexes

(A–C) Experimental 3.5 Å resolution $|F_{nati} - F_{RPN}|$ (A) (3.5σ level), and $|F_{RPN} - F_{nati}|$ (B) and $|F_{RFB} - F_{nati}|$ (C) (3.0σ level both) omit ED maps (green) superimposed on the RNAP1/Rifs structures.

(D) Superposition of the RPN (magenta) and RFB (green) atomic models. The RNAP1 structure is shown by the white ribbon diagram, the active-site Asp side chains (cyan) are represented by a balls-and-sticks model. In this and the following structural figures, the same color scheme is used for the RNAP subunits and the Rifs' atomic models: β—light yellow, β′—white, Rifs—pink.

both (Figure 3A), indicating that structural results obtained with *T. thermophilus* RNAP would be applicable to other bacterial species. RPN differs from RFP by only a few extra atoms that make no interactions with the protein, allowing for direct comparison between the ttRNAP/RPN(RFB) and taqRNAP/RFP complexes at the atomic level. Similar to those in the taqRNAP/RFP complex, most contacts in the ttRNAP/Rif complexes were observed between the β subunit residues and the ansa rings (Figures 3B and 3C). However, the network of the polar interactions with the ring system was much more extensive, comprising eighteen versus eight hydrogen bonds in the taqRNAP/RFP complex (Campbell et al., 2001), with three additional bonds made by σ in RNAP1 (Figures 3B and 3C and Figure 4A).

Numerous screens for Rif-resistant isolates have been performed, yielding important insights into rifampicin action (Jin and Gross, 1988; Romero et al., 1973; Severinov et al., 1993, 1994; Telenti et al., 1993); however, because of disparities in assay conditions and the scoring of the resistant phenotypes, we performed saturating mutagenesis of the *E. coli rpoB* regions associated with Rif resistance in vitro and in vivo to evaluate the contribution of each β residue in contact with Rif (Figure 3A). The crucial differences between the ttRNAP and taqRNAP polar contacts with Rifs involve βArg529, βGln513, and βHis526, which form three, four, and two hydrogen bonds with four Rif oxygen atoms in ttRNAP, respectively; only one such bond is formed by each of these residues in taqRNAP. These oxygen atoms are known to be essential for Rif inhibition (Bacchi et al., 1998) and are rigidly fixed by the Rifs' backbone. Furthermore, βArg529, βGln513, and βHis526 form additional polar contacts with each other, thus creating an intricate RNAP/Rifs recognition pattern (Figures 3B and 3C). Such a concerted mode of binding implies that the exclusion of a single interacting group (either in RNAP or Rifs) would not only eliminate its specific contacts but also would likely disturb the entire interaction network and lead to a dramatic loss in binding affinity. Underscoring their functional importance, substitutions of βArg529, βGln513, and βHis526 side chains for smaller ones conferred strong Rif resistance, whereas elimination of other RNAP/Rif polar interactions elicited smaller effects (Figure 3). The ttRNAP/Rif structures also revealed additional contacts of βArg143 and βGln510 with Rifs. Notably, the hydrogen bond between taqβAsp516 and O2 of Rif, which has been invoked to explain strong RFP resistance of the βAsp516 mutants, was not observed in the ttRNAP complexes and the substitution of the *E. coli* βAsp516 for Ala did not elicit strong RFP resistance (Figure 3A). These disparities could be attributed to the lower resolution of the taqRNAP/RFP structure; indeed, a brief analysis of the recently improved structure of taqRNAP/RFP complex (Campbell et al., 2005) indicates that both the overall taqRNAP structure and the Rif binding pocket resemble the ttRNAP conformation far more closely than the previously published taqRNAP/RFP complex (Campbell et al., 2001). In particular, the βAsp516/RFP hydrogen bond is also missing in the updated taqRNAP/RFP structure. However, significant differences in Rifs contacts still remain between the ttRNAP/Rifs and the improved taqRNAP/RFP structures.

The ttRNAP/RPN and ttRNAP/RFB complexes also revealed contacts between the antibiotics and the σ

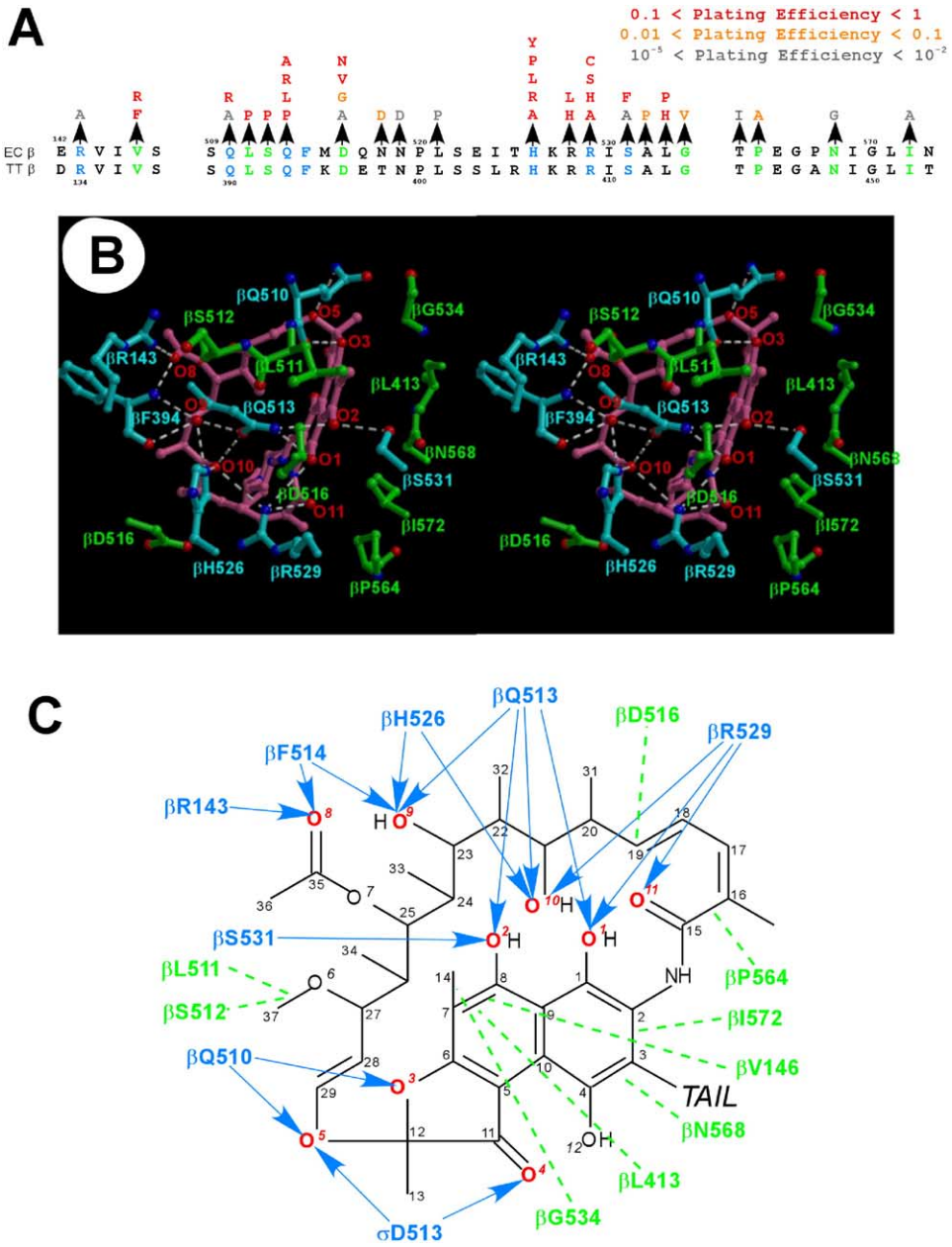

Figure 3. RNAP/Rifs Binding

Residues making polar (cyan) and hydrophobic (green) interactions with the Rifs' ansa ring are shown.

(A) The Rif-resistant substitutions characterized in this study are shown on top of the sequence alignment between *E. coli* and *T. thermophilus* β subunits.

(B and C) Three-dimensional stereo (RNAP1/RPN model was used) and schematic drawings show the RNAP/ansa ring hydrogen bonding using the cyan dashed lines or arrows, and the van der Waals contacts using green dashed lines.

subunit that were strikingly different in RNAP1 and RNAP2 (Figures 4A and 4B). In RNAP1, the σ hairpin loop (σHL, *E. coli* σ^{70} residues 508–519) closely approached bound Rifs while the σAsp513 side chain formed nearly identical hydrogen bonds with O4 and O5 of RPN and RFB. In RNAP2, the σHL was distant from the rings and interacted specifically with the RFB tail; in contrast, it formed only nonspecific van der Waals contacts with RPN. At the same time, the quality of the ED, nearly equal B factors, and nearly identical orientations suggest that RFB and RPN bind equally well to RNAP1 and RNAP2 and that their contacts with σHL contribute little to the binding affinity, a prediction which is supported by our biochemical data (see below). The proximal and distal orientations (with respect to the Rif binding site) of the σHL were observed in all previous ttRNAP structures and thus are likely unrelated to the Rif's binding, but rather may represent two

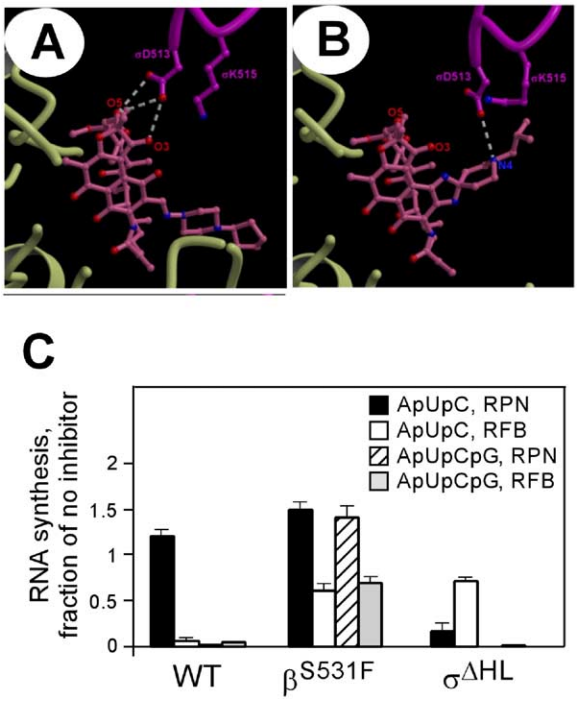

Figure 4. Interactions of the $\sigma^{\Delta HL}$ with Rifs and Effects on Transcription

(A and B) Interactions of the σHL (magenta) with the RPN/RFB ansa ring in RNAP1 (A) and with the RFB tail in RNAP2 (B).

(C) Effects of the $\sigma^{\Delta HL}$ and β^{S531F} substitution on ApUpCpG and ApUpC synthesis at the T7A1 promoter upon addition of RPN or RFB to 10 μg/ml. Data shown are the mean and SD (n = 3).

distinct physiologically relevant conformers that exist in dynamic equilibrium in the free holoenzyme. This equilibrium, however, could be shifted upon formation of the transcriptionally competent open complex in the presence of Rif.

The structural data allow us to draw one important conclusion: the differential effects of RPN and RFB on transcription cannot be adequately explained by the steric model. Indeed, the ansa rings of both RFB and RPN occupy the same site on RNAP and thus should sterically block the nascent RNA in identical fashion. Furthermore, as reported above, RPN blocks the second, while RFB inhibits the first bond formation; however, in the complex with RNAP, the RFB tail is located farther from the active site and thus farther from the growing RNA/DNA hybrid (Figure 2D), suggesting completely opposite effects in light of the steric model.

The RNAP/Rif complex models suggest several hypotheses that can be verified experimentally. *First*, since contacts of σHL with the RFB tail constitute the only difference in RNAP binding between RFB and RPN, σ could be responsible for distinct patterns of transcription inhibition by Rifs (Figure 1B). *Second*, binding of Rifs apparently leads to a loss of the catalytic Mg^{2+} ion from the active site (Figure 2A). As Rifs bind nearly 20 Å from the RNAP active site, this suggests that an allosteric signal culminating in Mg^{2+} displacement is transmitted from the Rif binding site to the catalytic Asp residues. Thus an increase in Mg^{2+} concentration should protect RNAP against inhibition by Rifs. Indeed, over 30 years ago such an effect was reported for RFP (Kerrich-Santo and Hartmann, 1974). *Third*, the structural data might allow us to trace the path along which the allosteric signal is transmitted, which then could be disrupted through engineered substitutions in RNAP.

Deletion of the σHL Has Distinct Effects on Inhibition by Rifs

Our structural data pointed to a rather dynamic nature of Rifs interactions with σHL, complicating assignment of the differential effects of RPN and RFB on transcription to a particular residue. Therefore, to test the first hypothesis, we deleted residues 507 through 519 in the σ^{70} subunit of *E. coli* RNAP ($\sigma^{\Delta HL}$) to eliminate all the interactions of σHL with Rifs. We predicted that this deletion, which does not confer gross transcriptional defects (Zenkin and Severinov, 2004), would not alter the common features of the RFB and RPN mechanisms (such as inhibition of the ApUpCpG synthesis) but could affect the RFB-specific inhibition of the first phosphodiester bond formation (ApUpC synthesis). Indeed, $\sigma^{\Delta HL}$ specifically conferred resistance of the ApUpC formation to RFB (Figure 4C): synthesis of ApUpC by the holoenzyme assembled from the wild-type core RNAP and $\sigma^{\Delta HL}$ was as efficient as ApUpC synthesis by the holoenzyme assembled from the β^{S531F} core (one of the strongest RFP-resistant substitutions known) and the wild-type σ^{70} but was inhibited by RFB during subsequent steps. In contrast, a deletion in the HL inhibited formation of the first bond in the presence of RPN (Figure 4B). Though we do not understand the basis for this observation, the effect of the HL deletion could explain the differential response to structurally homologous RFP of the holoenzymes with alternative σ factors, which likely have distinct conformations of σHL (Wegrzyn et al., 1998). On the other hand, in agreement with structural predictions, the $\sigma^{\Delta HL}$ holoenzyme bound to RFP as well as did the wild-type RNAP (Figure S2). Since σHL is located too far to interact directly with the nascent RNA/DNA hybrid, the apparent σ-dependent Rif effect on the first bond formation is likely caused by the allosteric σ-mediated signal that modulates catalysis and correlates with the loss of the active site Mg^{2+} ion.

Mg-Dependent Protection against Rifamycins

To test the second hypothesis, we ascertained whether Rif inhibition can be overcome by elevated Mg^{2+} levels. First, we studied survival of the *E. coli rpoB*^{N518D} cells in the presence of Rif as a function of Mg^{2+} concentration (Figure 5A). Addition of 25 mM $MgSO_4$ did not increase cell viability in the absence of inhibitor but rather led to a dramatic, 200-fold increase in the number of viable cells on RFP plates, whereas intermediate Mg concentrations produced lesser effects. Similar effects were observed in the presence of RPN or RFB and with several other *rpoB* alleles (data not shown). The increase in viability could be due to either the attenuated inhibition by RFP or a decrease in cell permeability to rifamycins. Control experiments demonstrated that the up-

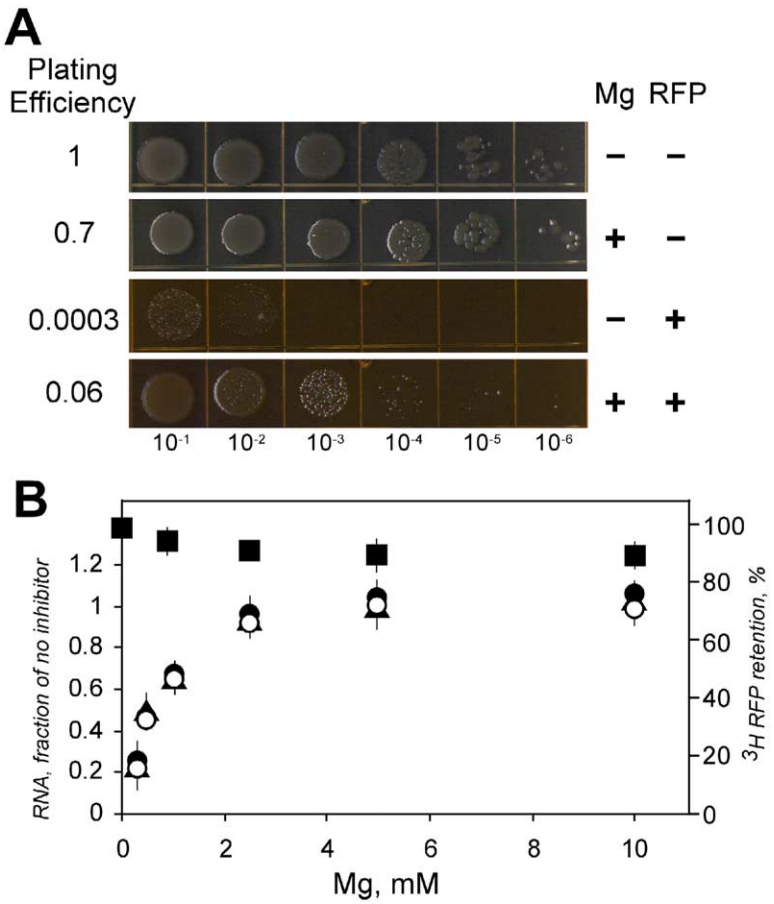

Figure 5. Increased Levels of Mg^{2+} Ion Protect RNAP against Inhibition by Rifs

(A) Mg-dependent survival of the *E. coli* cells carrying the plasmid-encoded IPTG-inducible *rpoB*^{N518D} allele (see Experimental Procedures) in the absence or in the presence of RFP (50 mg/l); $MgSO_4$ was added to 25 mM.
(B) Effect of Mg^{2+} concentration on RNA synthesis in the presence of Rifs and RFP binding in vitro. Synthesis of the halted A29 transcription complexes was measured on pIA171 template with 100 μM ApU, 2.5 μM GTP, 1 μM CTP, 10 μCi of [α^{32}P]-CTP (3000 Ci/mmol) at 37°C for 15 min in TGA buffer containing different concentrations of Mg^{2+}. Inhibition of A29 RNA synthesis by Rifs (relative to A29 synthesis in the absence of inhibitor, defined as 0% inhibition) was determined with RFB at 1 μg/ml (filled circles), RFP at 0.5 μg/ml (filled triangles), or RPN at 0.5 μg/ml (open circles). To determine retention of ^{3}H-labeled RFP (filled squares), stable initiation complexes were formed on pIA171 template during 15 min incubation at 37°C in the presence of 100 μM ApU; the concentration of Mg^{2+} was then adjusted between 0.4 and 10 mM and RFP retention was measured as described in Experimental Procedures. Binding at 0.4 mM Mg^{2+} was taken as 100%. Data shown are the average and spread of two measurements.

take of ^{3}H-labeled RFP did not vary over the same $MgSO_4$ range (data not shown). Second, we tested the effect of Mg titration on transcription by *E. coli* RNAP in vitro (Figure 5B). Increase of Mg^{2+} from 0.25 to 10 mM led to a decrease in inhibition of RNA synthesis by RPN or RFB from 80% to 0% (as compared to no Rif). Importantly, this protection is not absolute—elevated Mg^{2+} levels simply shift upward the inhibitory concentration of Rif and thus confer partial relief of inhibition in vivo and in vitro. This effect could be due to the displacement of RFP from the transcription complexes by Mg^{2+} ions. However, RFP binding to the initiation complexes did not change over the same range of Mg^{2+} concentrations (Figure 5B).

β-Mediated Allosteric Signal

The proposed σ-mediated signal explains the Rif-induced allosteric effect on the first bond formation. However, the $\sigma^{\Delta HL}$ RNAP is susceptible to inhibition at the consecutive steps, suggesting another allosteric pathway from the Rif binding to the RNAP active site. Apart from the already noted contacts with the σHL, the Rif binding site consists exclusively of β subunit residues. Over the years, many Rif-resistant *rpoB* mutants were isolated as a result of mutagenesis and selection or during analysis of clinical samples. While the majority of substitutions occurred at positions involved in direct contact with the rifamycin body, several variants, such as D516V, N519K, S522L, or R687H, do not fall into this category. Interestingly, the first three mutants (the fourth was not tested) are resistant to RFP but very sensitive and thus still bind to RFB (Wichelhaus et al., 2001; Williams et al., 1998). Since the altered residues cluster on the side of the invariant ansa ring that lies opposite the tail, their effects cannot be easily explained by the earlier proposal that Rif resistance always stems from a loss of binding to a distorted Rif binding pocket (Campbell et al., 2001). Of these residues only βAsp516 is located within the interacting distance with Rifs in the ttRNAP/Rif structures. It, however, makes only weak van der Waals interactions with the Rifs' backbone (Figures 3B and 3C); thus substitutions to a smaller Val or isosteric Asn should not dramatically affect the Rif affinity. Indeed, these substitutions conferred strong resistance to RFP in vivo while retaining sensitivity to RFB in vivo and significant binding (~25% of wild-type RNAP) to RFP in vitro (Figure 3A and Supplemental Data, Binding of RFP to RNAP Variants and Figure S2). In contrast, three RNAP variants that displayed a dramatic loss of RFP binding (3%–5% of wild-type RNAP; Figure 3A and Supplemental Data, Binding of RFP to RNAP Variants and Figure S2) were substantially more sensitive (10- to 1000-fold) to RFP than $\beta^{D516V/N}$ enzymes. Two of these variants (as well as the $\beta^{D516V/N}$ RNAP mutants) did not confer significant growth defects in the absence of antibiotics, thereby

suggesting that their strong resistance to RFP (equal to that of $\beta^{D516V/N}$) cannot be attributed solely to the lower viability (see details in Supplemental Data, Binding of RFP to RNAP Variants). Together, these observations suggest that βAsp516 affects Rif action allosterically. Taking βAsp516 as a reference, we have traced a putative pathway from this residue toward the active site. Remarkably, βArg687 (Thr in *T. thermophilus*), which has direct contacts with βAsp516 and whose substitution to His is RFP resistant (Jin and Gross, 1988), lies in this path (Figure 6A). Other residues include βMet685 and βLeu1235, which form a hydrophobic core with βLys1066 and βLys1074, the latter two residues making direct contacts to the active site loop. We constructed a β^{L1235A} variant that lies in the putative signal transduction pathway far away from both the Rif binding and active sites. To provide further validation of the modeled allosteric pathway, we also substituted two other residues (β^{N684A} and β^{M681A}) that are located near βLeu1235 and at approximately the same distance from the Rif binding site but do not contribute to the network of interactions allosterically linking the Rif binding and active sites.

According to our expectations, we found that β^{L1235A} supported *E. coli* growth in the presence of RFP, whereas the other two "off-pathway" variants did not (Figure 6B and data not shown). Although the RFP-resistant mutant grew slowly in the presence and absence of inhibitors, the slow growth per se was insufficient to confer RFP resistance: two β variants that contained substitutions of residues 1105 and 1106 distant from both the RFP binding pocket and the allosteric pathway grew equally slowly but remained sensitive to RFP (Figure 6B). We purified β^{L1235A} RNAP and showed that while it was resistant to RFP inhibition in vitro, its affinity was even higher than that of the wild-type RNAP, in contrast to RFP-resistant β^{Q513P} enzyme that did not retain the inhibitor above the background level (Figure 6C). These data support the hypothesis that the βLeu1235 residue is necessary to transmit the allosteric signal but is dispensable for Rif binding.

Mechanism of Inhibition of Transcription by Rifamycins

Altogether our data suggest that Rif binding to RNAP induces an allosteric signal that is transmitted to the RNAP active site and disfavors binding of the major catalytic Mg^{2+} ion. The loss of the Mg^{2+} ion slows down the reaction, which in turn likely results in spontaneous dissociation of the short, unstable RNA/DNA hybrids (Schulz and Zillig, 1981). Although we do not rule out the steric block as a component of the inhibition mechanism, the steric block alone seems insufficient to inhibit transcription: both Mg^{2+} and certain RNAP substitutions ($\beta^{D516V/N}$, $\sigma^{\Delta HL}$, and β^{L1235A}) confer resistance to RFP but do not eliminate the binding of antibiotic, which presumably is still bound in the path of growing RNA.

Our data are consistent with the existence of at least two allosteric pathways from Rif to the RNAP active site: the σ pathway affects the first, whereas the β pathway modulates the second/third phosphodiester bond formation. Activation of the σ pathway is apparently dependent on the orientation of the Rif tail. Indeed, RFB, whose tail has unique contacts with σHL, blocks the first bond formation, thereby relying largely on the σ pathway. Truncation of σHL, which likely disturbs the σ pathway, restores the first bond formation in the presence of RFB. At the same time, σ deletion had no effect on the inhibition of the second bond by either Rif. In turn, mutations that disrupt the β pathway (β^{D516V}) conferred resistance to RFP, which inhibits only the second, but not the first, bond formation, while retaining sensitivity to RFB (Wichelhaus et al., 2001; Williams et al., 1998).

The allosteric mechanism proposed here resolves practically all the discrepancies between the proposed steric mechanism and functional studies of Rif inhibition. In particular, it explains the differential response of some *rpoB* mutants to Rifs in vivo, effects of Rif tails on transcription in vitro, and the differential RFP resistance of the holoenzymes with alternative σ factors (Wegrzyn et al., 1998). Finally, the RFP-induced loss of the catalytic Mg^{2+} ion, rather than a simple steric hindrance of the RNA extension, helps to provide a unified explanation to a seemingly unrelated and surprising set of observations, such as (1) inhibition by RFP of RNA synthesis and transcript cleavage (both are Mg^{2+} dependent) in the binary complexes (Altmann et al., 1994), (2) relief of RFP-dependent inhibition by elevated Mg^{2+} (Figure 5 and Kerrich-Santo and Hartmann, 1974), and (3) potentiation of RFP effects in vivo by treating cells with Mg^{2+}-chelating EDTA and EGTA (Sarubbi et al., 2004).

Propagation of the allosteric signal likely involves nucleic acid components of the transcription initiation complex. Our model of the open complex (Artsimovitch et al., 2004) suggests that σHL likely interacts with the template DNA strand, which may therefore participate in the σ pathway. Subtle alterations of the same model show that 5′ NTP (or NMP) in the *n-3* position of the RNA transcript (second bond formation) does not necessarily clash with bound Rif, as was suggested earlier (Campbell et al., 2001). Instead, its tri-phosphate (monophosphate) moiety may make contacts with βArg529, βArg687 and βThr525 (Thr and Arg in *T. thermophilus*, respectively), and βAsp516 (Figure 6A). Their additional interactions with 5′ RNA tri-/mono-phosphate might be essential to "switch on" the allosteric signal in the β pathway. In contrast, the 5′-terminal RNA nucleotide at the *n-2* position (first bond formation) would be too far away to form similar modulatory contacts with the Rif binding site residues. As a result, the allosteric modulation of the active site destabilizing catalytic Mg^{2+} ion would not occur, thereby explaining why the β pathway inhibits the second but not the first bond formation. It is, however, worth noting that the proposed β pathway mechanism is hypothetical and a more specific analysis is required to elucidate its details.

Another important question is the exact mechanism by which the Rif-induced allosteric signal leads to the reduced affinity for the principal Mg^{2+} ion in the active site. We do not observe large systematic conformational changes in the active site upon Rifs' binding that could exclude Mg^{2+} ion sterically and/or compromise Mg^{2+} coordination bonds by moving apart the active-site Asp side chains. In contrast, in all four RNAP mole-

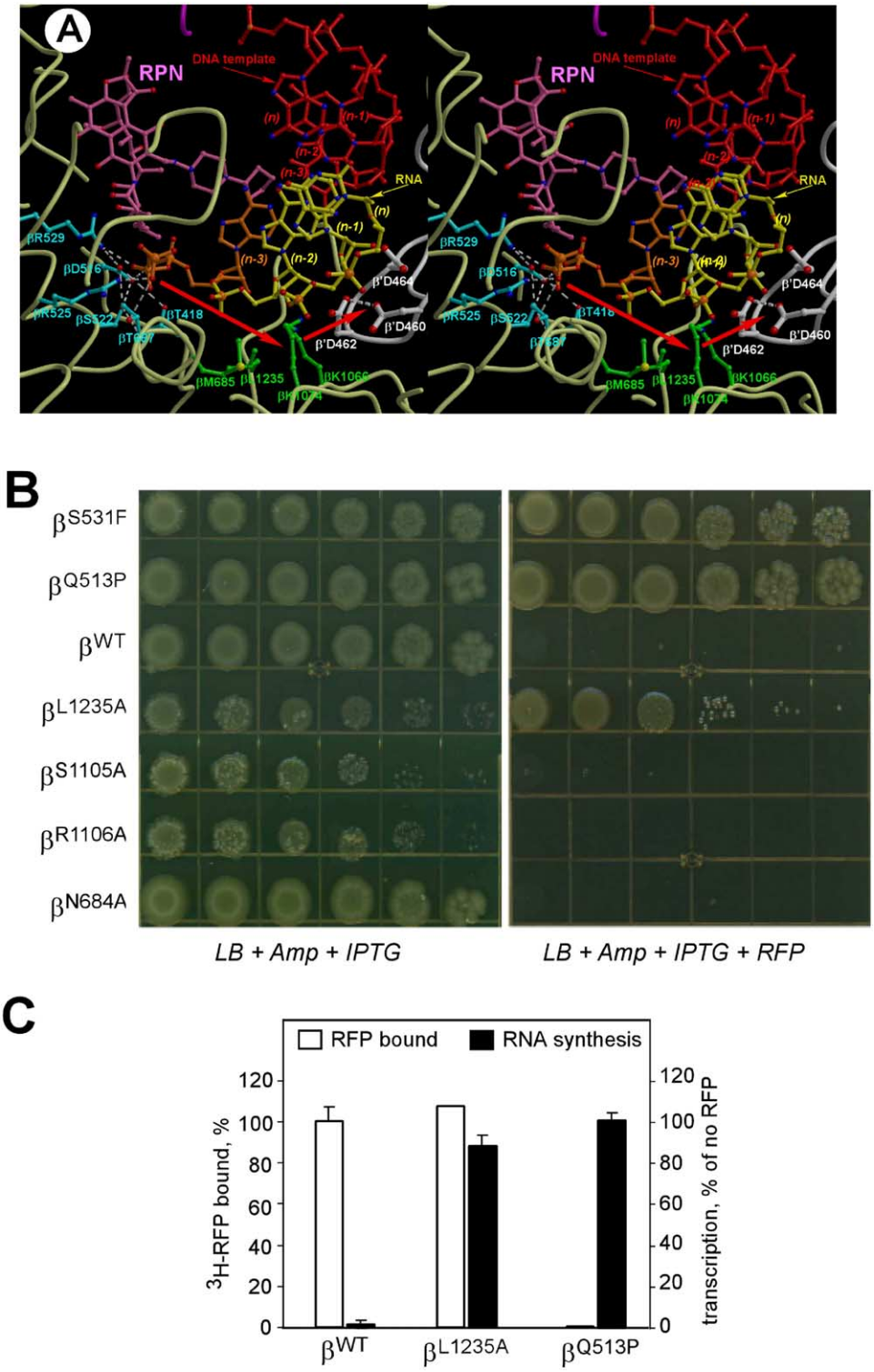

Figure 6. β Subunit-Mediated Allosteric Signal

(A) A putative three-dimensional trace (stereo) of the signal (red arrows) that originates from the set of polar residues in the Rif binding site (cyan) and is transmitted to the active site (white) through the intervening hydrophobic cluster (green). A model of the 4 bp (second bond is formed) RNA/DNA hybrid (yellow/red) with the 5′-terminal RNA NTP (orange) is superimposed on the RNAP/RPN structure.

(B) Substitutions that disrupt Rif binding (β^{Q513P}, β^{S531F}) and the allosteric pathway (β^{L1325A}) grow in the presence of RFP. Serial dilutions of IPTG-induced cultures were plated on LB-Amp-IPTG in the absence and in the presence of 20 mg/l RFP and grown at 32°C. Pictures were taken after 43 hr incubation.

(C) Both β^{Q513P} and β^{L1325A} enzymes are resistant to RFP in vitro, but only β^{L1325A} retains RFP binding. Transcription was assayed on a T7A1 promoter encoded on a pIA171 template in the absence and in the presence of 2 μg/ml RFP, as described in the Figure 5 legend. Binding was assayed as described in Experimental Procedures. Data shown are the mean and SD (n = 3).

cules in the complex structures, the side chains of β′Asp460 and β′Asp464 are brought together somewhat closer than in the apo-holoenzyme, at a distance of ~2.4–2.55 Å (Figure 6A), suggesting their protonation and a strong hydrogen bond formed between these residues in the presence of Rifs. The evidence for such hydrogen bonding was provided by the extra-high-resolution (0.97 Å) structure of the periplasmic phosphate receptor, in which two protonated acidic groups (Asp and phosphate) form a hydrogen bond with unusually short distance (~2.4 Å) (Wang et al., 1997). Other systematic conformational differences between the RNAP/Rif complexes and the apo-holoenzyme involve the side chains in the Rif binding site. The most notable are the altered positions of the βArg529 and βAsp516 side chains, which in all Rif complexes form a stable hydrogen bond missing in the apo-holoenzyme structure (Figure 6A), thereby inducing changes in the extensive interaction network and likely in the overall charge distribution in the vicinity of the Rif binding (Figure 6A); these charge alterations might be then transmitted further to change the local pK_as of the RNAP active site residues with no significant structural alterations of the RNAP backbone and side chains. Consistently, the β^{D516N} substitution, which changes the chemical but not steric properties of the side chain, confers strong Rif resistance (Figure S2). We speculate that the allosteric signal may result in protonation of the active-site acidic residue(s) to favor the Asp-Asp hydrogen bonds that would compromise the catalytic Mg^{2+} binding.

Perspectives for Drug Design

The major problem in the clinical use of rifamycins (and other antibiotics) is the rapid spread of bacteria bearing resistant mutations; in the case of Rifs, the vast majority of these mutations map to the *rpoB* gene. The functional analysis of Rif action in combination with the high-resolution structural data illuminated the detailed RNAP/Rif interaction network at the atomic level and revealed the crucial determinants of Rif binding in both RNAP and Rifs. These data provide structural and mechanistic guidelines for development of new and improved Rif derivatives.

Analysis of the Rif-resistant variants (Figure 3) shows that they fall into three categories: (1) "steric" mutants, which reduce space in the Rif binding site and exclude Rif through a steric clash with its backbone; (2) "affinity" mutants, which remove crucial protein polar/hydrophobic contacts with Rif; and (3) "allosteric" mutants, which interfere with the transmission of the Rif-induced allosteric signal. Importantly, three positions altered in ~85% of clinical isolates represent all three categories: $\beta^{S531L,F,Y}$—steric, β^{H526X}—affinity, and $\beta^{D516V,G}$—allosteric (Figure 3; Table S1).

Most steric mutants attack the Rif portion consisting of three planar rings, which cannot adopt any alternative conformation and are therefore exceedingly inflexible. Moreover, this substructure defines to a large extent the overall Rif conformation. Thus, one apparent way to decrease sensitivity to steric mutations is to replace the ring portion of Rif with a more flexible structure retaining all the necessary hydrogen bonding determinants (O1, O2, O11) to make the inhibitor sterically self-adjustable to bulky substitutions in the protein, which would substantially modify the conformational profile of the binding site. Indeed, the antibiotic sorangicin, which occupies the Rif binding site and mimics the overall Rif conformation while lacking the Rif planar rings and thus being more flexible, retains sensitivity toward a number of the Rif-resistant steric RNAP mutants (Campbell et al., 2005).

To decrease the effect of the affinity mutants, Rif derivatives with additional groups that would provide extra contacts with the protein could be constructed. To minimize the impact of specific RNAP steric and affinity substitutions, these derivatives should bear polar groups that would form hydrogen bonds with the RNAP main chain atoms, or flexible hydrophobic groups that would rely on nonspecific van der Waals interactions. Our structural analysis allows us to suggest two such modifications. First, the negatively charged pocket (β506–513) exposing four main chain carbonyl oxygens may bind to an additional Rif group with the complementary positive charge attached to C27. Second, the hydrophobic cavity formed by βMet459, βPhe505, βLeu511, and βPro535 may accommodate a hydrophobic tail attached to C14.

Development of antibiotic derivatives that may compensate for the allosteric mutations is not apparent from the structure and may therefore require an extensive trial-and-error approach. However, our finding of the σ pathway that likely relies on the Rif interactions exclusively with the σ subunit σHL may substantially facilitate the design of the allosterically insensitive compounds. The σ pathway is better protected against allosteric resistance than the β pathway, as all bacteria encode several σ factors and simultaneous appearance of Rif-resistant mutations in several genes is unlikely. Indeed, all known Rif-resistant mutants are located in the β subunit. Thus, construction of Rif derivatives that would amplify the signal in the σ pathway looks highly promising.

Concluding Remarks

RNAP is a powerful molecular motor that generates a force of ~14 pN (Yin et al., 1995). An excellent illustration of its power is transcription initiation, in which a growing RNA/DNA hybrid displaces a large protein, the σ subunit that binds to the core enzyme with nanomolar affinity (Gill et al., 1990) forming an extensive interface through multiple polar and hydrophobic interactions (Vassylyev et al., 2002). It is not immediately clear why a proposed collision with a much smaller Rif molecule having similar binding affinity (Barh et al., 1976) would be a much stronger antagonist of the nascent RNA/DNA hybrid extension. On the other hand, if the Rif-induced allosteric signal compromises the catalytic Mg^{2+} ion binding it could affect inhibition of transcription even before the RNA/DNA hybrid is long enough to collide with RNAP bound Rif (as can be the case with inhibition of the first phosphodiester bond by RFB). As a weak Lewis acid, Mg^{2+} is ideally suited for catalysis of phosphodiester bond formation, while precise coordination by invariant Asp residues accounts for much of the stereo- and enantioselectivity of the catalyzed

reaction—thus even slight alterations of the Mg^{2+} ion position could trigger a switch between different catalytic pathways, for example, from nucleotide addition to exonucleolytic cleavage. Repositioning of the Mg^{2+} ions in vicinity of the active site has recently emerged as a common theme in regulation of RNAP by extrinsic factors (Nickels and Hochschild, 2004); our data suggest that transcriptional inhibitors may utilize similar regulatory mechanisms.

Experimental Procedures

Structure Determination and Refinement

The ttRNAP holoenzyme was purified and crystallized as described previously with the only exception that the pH value was slightly shifted as compared to the previous crystallization conditions (from 5.8 to 6.5) (Artsimovitch et al., 2004; Vassylyev et al., 2002; Vassylyeva et al., 2002). To obtain the complex crystals, the crystals of the apo-holoenzyme were transferred for 4 hr into the drops containing harvest buffer and 2 mM of RPN or RFB. The data for apo-holoenzyme and the ttRNAP/RFB and ttRNAP/RPN complexes were collected at the beam line BL5 at Photon Factory (Tsukuba, Japan) using ADSC Quantum-315 CCD detector. All the crystals, though belonging to the same space group, $P3_2$, exhibited somewhat distinct unit cell parameters, a = b = 240 Å, c = 253 Å, as compared to the previously studied ttRNAP crystals (a = b = 236 Å, c = 250 Å) (Vassylyeva et al., 2002). The data were processed using HKL2000 data processing package (Otwinowski and Minor, 1997). The refinement was carried out using the CNS program (Brunger et al., 1998). The RPN and RFB models were built into the initial experimental difference ED map (Figures 2C and 2D). The rigid body refinement followed by several rounds of the B factor, positional, simulated annealing refinements and water "pick" and water "delete" procedures, alternating by manual model building using the O program (Jones et al., 1991), yielded the final R factors of 23.1%, 23.0%, and 22.5% and R_{free} of 26.8%, 26.7%, and 25.7% for the apo-holoenzyme, ttRNAP/RPN, and ttRNAP/RFB complexes, respectively (Table 2). The final models were of high quality as revealed by the simulated annealing omit ED maps calculated for RPN and RFB (Figure S1). Three-dimensional structural figures were prepared using programs Molscript (Kraulis, 1991), Bobscript (Esnouf, 1999), and Raster3D (Merrit and Bacon, 1997).

Plating Efficiency Test

Overnight cultures of *E. coli* DH5α strain transformed with plasmids encoding different *rpoB* variants under control of IPTG-inducible P_{trc} promoter grown in LB supplemented with 100 mg/l ampicillin (Amp) were diluted 50-fold into fresh LB+Amp and grown to OD_{600} of 0.3 at 37°C. IPTG was added to 1 mM for 1.5 hr at 37°C (to allow incorporation of the plasmid-encoded β into RNAP), and serial tenfold dilutions were made and spotted (in 7 μl drops) on LB plates supplemented with Amp (100 mg/l) and IPTG (1 mM). Different rifamycins (or an equal volume of 50% ethanol) were added to 50 mg/l. $MgSO_4$ was added where indicated. Plates were incubated at 32°C for 24 to 72 hr. The plating efficiency was calculated as the ratio of viable cells grown on the plate supplemented with rifamycin to that on the control plate (LB + Amp + IPTG). Plating efficiencies were determined at least three times for each *rpoB* mutant under the specified condition.

rpoB Mutagenesis and Core RNAP Purification

Desired mutations were introduced by site-directed mutagenesis into the plasmid-encoded *rpoB* gene placed under control of IPTG-inducible P_{trc} promoter (pIA545 or pIA160). Random mutagenesis was performed during PCR amplification with Taq DNA polymerase in the presence of 0.5 mM $MnCl_2$, followed by screening on LB + Amp + IPTG plate supplemented with rifamycins. The region surrounding each substitution was sequenced and transferred back into the unmutagenized plasmid background. To create the expression vectors, NcoI-SdaI fragments of mutant *rpoB* genes were recloned into pIA509 vector, which encodes the *rpoA-rpoB-rpoC* gene cassette placed under control of T7 gene10 promoter (Artsimovitch et al., 2003); the β subunit carries an N-terminal hexahistidine tag. All plasmids used in this work are listed in Table S2. Core RNAP-containing β substitutions were purified from a DH5α strain transformed with pIA545 and derivative plasmids upon induction with IPTG, followed by chromatography on Ni-NTA (Qiagen), Heparin HiTrap, and Q FF-sepharose columns using ACTA Prime LC chromatography system (GE Healthcare). Core RNAP from pIA509-derivative plasmids were purified from DH5α/λDE3 strain through the same chromatographic steps. All proteins were dialyzed into RNAP storage buffer (10 mM Tris, pH 7.9, 50% glycerol, 0.1 mM EDTA, 0.1 mM DTT, 0.1 M NaCl) and stored at −20°C or −80°C.

rpoD Mutagenesis and σ Subunit Purification

$\sigma^{\Delta 507\text{-}519}$ was constructed by site-directed mutagenesis. The mutagenized region was sequenced and recloned into pIA586 to generate pIA582. Wild-type σ was purified from BL21/λDE3 transformed with $pET\sigma^{70}$ under denaturing conditions (Marr and Roberts, 1997) using a combination of Ni-NTA agarose and heparin column chromatography; $\sigma^{\Delta 507\text{-}519}$ was purified from pIA582 similarly.

In Vitro Transcription

All templates for transcription reactions were generated by PCR amplification. Holoenzymes containing wild-type or substituted β or σ subunits were assembled from core RNAP and σ (1:2 molar ratio) for 20 min at 32°C in storage buffer. To form an open complex, linear DNA template (2 nM) and RNAP holoenzyme (50 nM) were incubated at 37°C for 15 min in TGA buffer (20 mM Tris-acetate, 20 mM Na-acetate, 5% glycerol, 14 mM 2-mercaptoethanol, 2 mM Mg-acetate, 0.1 mM EDTA, pH 8.0) unless noted otherwise. Then rifamycins were added for 1 min, followed by incubation with substrates, 100 μM ApU, 2.5 μM GTP, 1 μM CTP, 10 μCi of [α^{32}P]-CTP (3000 Ci/mmol), at 37°C for 10–20 min. Reactions were terminated by the addition of an equal volume of STOP buffer (10 M urea, 20 mM EDTA, 45 mM Tris-borate; pH 8.3), analyzed by denaturing gel electrophoresis, visualized using Storm820 (GE Healthcare), and quantified with Microsoft Excel or KaleidaGraph.

RFP Binding Assays

H^3-labeled RFP (26.8 Ci/mmol, Moravek Biochemicals, Brea, California) was mixed with *E. coli* RNAP holoenzymes (2 nM RFP to 10 nM RNAP) or initiation complexes in 1× TGA transcription buffer and incubated at 37°C for 15 min. Five hundred microliters of the binding reaction were loaded onto VivaSpin-500 100K filter and concentrated ~10×. The mix was washed twice with nine volumes of binding buffer; the final retentate in case of negative control (heat-denatured RNAP) contained <0.5% of the loaded radioactivity. Final retentate radioactivity was quantified using a liquid scintillation counter. To evaluate effects of Mg^{2+} on RFP binding, EDTA was omitted from the buffer and concentration of $MgCl_2$ was adjusted to cover a 0.4–10 mM range both in the binding and wash buffers.

Supplemental Data

Supplemental Data include text, three figures, two tables, and references and can be found with this article online at http://www.cell.com/cgi/content/full/122/3/351/DC1/.

Acknowledgments

We are grateful to Dr. S. Yokoyama for his interest and support. We thank Drs. W.T. McAllister and M. Anikin for critical reading of the manuscript and the anonymous reviewers for insightful comments. This work was supported in part by National Institutes of Health grants AI64819 and GM67153 to I.A. and GM74252 to D.G.V. and by a RIKEN grant (to D.G.V.).

Received: March 22, 2005
Revised: May 15, 2005
Accepted: July 5, 2005
Published: August 11, 2005

References

Altmann, C.R., Solow-Codero, D.E., and Chamberlin, M. (1994). RNA cleavage and chain elongation by *Escherichia coli* DNA-

dependent RNA polymerase in a binary enzyme:RNA complex. Proc. Natl. Acad. Sci. USA *91*, 3784–3788.

Artsimovitch, I., Svetlov, V., Murakami, K.S., and Landick, R. (2003). Co-overexpression of Escherichia coli RNA polymerase subunits allows isolation and analysis of mutant enzymes lacking lineage-specific sequence insertions. J. Biol. Chem. *278*, 12344–12355.

Artsimovitch, I., Patlan, V., Sekine, S., Vassylyeva, M.N., Hosaka, T., Ochi, K., Yokoyama, S., and Vassylyev, D.G. (2004). Structural basis for transcription regulation by alarmone ppGpp. Cell *117*, 299–310.

Bacchi, A., Pelizzi, G., Nebuloni, M., and Ferrari, P. (1998). Comprehensive study on structure-activity relationships of rifamycins: discussion of molecular and crystal structure and spectroscopic and thermochemical properties of rifamycin O. J. Med. Chem. *41*, 2319–2332.

Barh, W., Stender, W., Scheit, K.H., and Jovin, T.M. (1976). Binding of rifampicin to Escherichia coli RNA polymerase: Thermodynamic and kinetic studies. In RNA Polymerase, R. Losick and M. Chamberlin, eds. (New York: Cold Spring Harbor), pp. 369–396.

Boyd, D.H., and Zillig, W. (1974). Reference mutations for the beta subunit of RNA polymerase. Mol. Gen. Genet. *130*, 315–320.

Brufani, M., Cellai, L., Cerrini, S., Fedeli, W., Segre, A., and Vaciago, A. (1982). Structure-activity relationships in the ansamycins. Molecular structure and activity of 3-carbomethoxy rifamycin S. Mol. Pharmacol. *21*, 394–399.

Brunger, A.T., Adams, P.D., Clore, G.M., DeLano, W.L., Gros, P., Grosse-Kunstleve, R.W., Jiang, J.S., Kuszewski, J., Nilges, M., Pannu, N.S., et al. (1998). Crystallography & NMR system: A new software suite for macromolecular structure determination. Acta Crystallogr. *D54*, 905–921.

Campbell, E.A., Korzheva, N., Mustaev, A., Murakami, K., Nair, S., Goldfarb, A., and Darst, S.A. (2001). Structural mechanism for rifampicin inhibition of bacterial rna polymerase. Cell *104*, 901–912.

Campbell, E.A., Pavlova, O., Zenkin, N., Leon, F., Irschik, H., Jansen, R., Severinov, K., and Darst, S.A. (2005). Structural, functional, and genetic analysis of sorangicin inhibition of bacterial RNA polymerase. EMBO J. *24*, 674–682.

Cramer, P., Bushnell, D.A., and Kornberg, R.D. (2001). Structural basis of transcription: RNA polymerase II at 2.8 angstrom resolution. Science *292*, 1863–1876.

Esnouf, R.M. (1999). Further additions to MolScript version 1.4, including reading and contouring of electron-density maps. Acta Crystallogr. *D55*, 938–940.

Floss, H.G., and Yu, T.W. (2005). Rifamycin-mode of action, resistance, and biosynthesis. Chem. Rev. *105*, 621–632.

Gill, S., Weitzel, S., and von Hippel, P. (1990). Escherichia coli sigma 70 and NusA proteins. I. Binding interactions with core RNA polymerase in solution and within the transcription complex. J. Mol. Biol. *220*, 307–324.

Jin, D.J., and Gross, C.A. (1988). Mapping and sequencing of mutations in the Escherichia coli rpoB gene that lead to rifampicin resistance. J. Mol. Biol. *202*, 45–58.

Jones, T.A., Zou, J.Y., Cowan, S.W., and Kjeldgaard, A. (1991). Improved methods for building protein models in electron density maps and the location of errors in these models. Acta Crystallogr. *A47*, 110–119.

Kawai, M., Ishihama, A., and Yura, T. (1976). RNA polymerase mutants of Escherichia coli. III. A temperature-sensitive rifampicin-resistant mutant. Mol. Gen. Genet. *143*, 233–241.

Kerrich-Santo, R.E., and Hartmann, G.R. (1974). Influence of temperature on the action of rifampicin on RNA polymerase in presence of DNA. Eur. J. Biochem. *43*, 521–532.

Kraulis, P.J. (1991). MOLSCRIPT: a program to produce both detailed and schematic plots of protein structures. J. Appl. Crystallogr. *24*, 946–950.

Maggi, N., Pallanza, R., and Sensi, P. (1965). New derivatives of rifamycin SV. Antimicrob. Agents Chemother. *5*, 765–769.

Marr, M.T., and Roberts, J.W. (1997). Promoter recognition as measured by binding of polymerase to nontemplate strand oligonucleotide. Science *276*, 1258–1260.

McClure, W.R., and Cech, C.L. (1978). On the mechanism of rifampicin inhibition of RNA synthesis. J. Biol. Chem. *253*, 8949–8956.

Merrit, E.A., and Bacon, D.J. (1997). Raster3D: photorealistic molecular graphics. Methods Enzymol. *277*, 505–524.

Mustaev, A., Zaychikov, E., Severinov, K., Kashlev, M., Polyakov, A., Nikiforov, V., and Goldfarb, A. (1994). Topology of the RNA polymerase active center probed by chimeric rifampicin-nucleotide compounds. Proc. Natl. Acad. Sci. USA *91*, 12036–12040.

Nickels, B.E., and Hochschild, A. (2004). Regulation of RNA polymerase through the secondary channel. Cell *118*, 281–284.

Otwinowski, Z., and Minor, W. (1997). Processing X-ray diffraction data collected in oscillation mode. Methods Enzymol. *276*, 307–326.

Ovchinnikov, Y.A., Monastyrskaya, G.S., Guriev, S.O., Kalinina, N.F., Sverdlov, E.D., Gragerov, A.I., Bass, I.A., Kiver, I.F., Moiseyeva, E.P., Igumnov, V.N., et al. (1983). RNA polymerase rifampicin resistance mutations in Escherichia coli: sequence changes and dominance. Mol. Gen. Genet. *190*, 344–348.

Romero, E., Riva, S., Berti, M., Fietta, A.M., and Silvestri, L.G. (1973). Pleiotropic effects of a rifampicin-resistant mutation in E. coli. Nat. New Biol. *246*, 225–228.

Sarubbi, E., Monti, F., Corti, E., Miele, A., and Selva, E. (2004). Mode of action of the microbial metabolite GE23077, a novel potent and selective inhibitor of bacterial RNA polymerase. Eur. J. Biochem. *271*, 3146–3154.

Schulz, W., and Zillig, W. (1981). Rifampicin inhibition of RNA synthesis by destabilisation of DNA-RNA polymerase-oligonucleotide-complexes. Nucleic Acids Res. *9*, 6889–6906.

Severinov, K., Soushko, M., Goldfarb, A., and Nikiforov, V. (1993). Rifampicin region revisited. New rifampicin-resistant and streptolydigin-resistant mutants in the beta subunit of *Escherichia coli* RNA polymerase. J. Biol. Chem. *268*, 14820–14825.

Severinov, K., Soushko, M., Goldfarb, A., and Nikiforov, V. (1994). RifR mutations in the beginning of the Escherichia coli rpoB gene. Mol. Gen. Genet. *244*, 120–126.

Sippel, A.E., and Hartmann, G.R. (1970). Rifampicin resistance of RNA polymerase in the binary complex with DNA. Eur. J. Biochem. *16*, 152–157.

Stender, W., Stutz, A.A., and Scheit, K.H. (1975). The modification of DNA-dependent RNA polymerase from Escherichia coli by an alkylating derivative of rifamycin SV. Eur. J. Biochem. *56*, 129–136.

Telenti, A., Imboden, P., Marchesi, F., Lowrie, D., Cole, S., Colston, M.J., Matter, L., Schopfer, K., and Bodmer, T. (1993). Detection of rifampicin-resistance mutations in Mycobacterium tuberculosis. Lancet *341*, 647–650.

Vassylyev, D.G., Sekine, S., Laptenko, O., Lee, J., Vassylyeva, M.N., Borukhov, S., and Yokoyama, S. (2002). Crystal structure of a bacterial RNA polymerase holoenzyme at 2.6 A resolution. Nature *417*, 712–719.

Vassylyeva, M.N., Lee, J., Sekine, S.I., Laptenko, O., Kuramitsu, S., Shibata, T., Inoue, Y., Borukhov, S., Vassylyev, D.G., and Yokoyama, S. (2002). Purification, crystallization and initial crystallographic analysis of RNA polymerase holoenzyme from Thermus thermophilus. Acta Crystallogr. D Biol. Crystallogr. *58*, 1497–1500.

Wang, Z., Luecke, H., Yao, N., and Quiocho, F.A. (1997). A low energy short hydrogen bond in very high resolution structures of protein receptor–phosphate complexes. Nat. Struct. Biol. *4*, 519–522.

Wegrzyn, A., Szalewska-Palasz, A., Blaszczak, A., Liberek, K., and Wegrzyn, G. (1998). Differential inhibition of transcription from sigma70- and sigma32-dependent promoters by rifampicin. FEBS Lett. *440*, 172–174.

Wehrli, W., and Staehelin, M. (1969). The rifamycins--relation of chemical structure and action on RNA polymerase. Biochim. Biophys. Acta *182*, 24–29.

Wichelhaus, T., Schafer, V., Brade, V., and Boddinghaus, B. (2001). Differential effect of rpoB mutations on antibacterial activities of rifampicin and KRM-1648 against Staphylococcus aureus. J. Antimicrob. Chemother. *47*, 153–156.

Williams, D.L., Spring, L., Collins, L., Miller, L.P., Heifets, L.B., Gan-

gadharam, P.R., and Gillis, T.P. (1998). Contribution of rpoB mutations to development of rifamycin cross-resistance in Mycobacterium tuberculosis. Antimicrob. Agents Chemother. *42*, 1853–1857.

Yin, H., Wang, M., Svoboda, K., Landick, R., Block, S., and Gelles, J. (1995). Transcription against an applied force. Science *270*, 1653–1657.

Zenkin, N., and Severinov, K. (2004). The role of RNA polymerase sigma subunit in promoter-independent initiation of transcription. Proc. Natl. Acad. Sci. USA *101*, 4396–4400.

Accession Numbers

The coordinates and structure factors for crystal structures of the RNAP apo-holoenzyme and its complexes with RPN and RFB have been deposited in the Protein Data Bank under ID codes 2A6E, 2A69, and 2A68, respectively.